

---

---

STATISTICAL, NONLINEAR,  
AND SOFT MATTER PHYSICS

---

---

## Shock-Wave Pressure Transfer to a Solid Target with Porous Absorber of High-Power Laser Pulse

I. A. Belov<sup>a</sup>, S. A. Bel'kov<sup>a</sup>, S. V. Bondarenko<sup>a</sup>, G. A. Vergunova<sup>b</sup>, A. Yu. Voronin<sup>a</sup>, S. G. Garanin<sup>a</sup>,  
S. Yu. Golovkin<sup>a</sup>, S. Yu. Gus'kov<sup>b</sup>, N. N. Demchenko<sup>b</sup>, V. N. Derkach<sup>a</sup>, E. O. Dmitriev<sup>b</sup>,  
N. V. Zmitrenko<sup>c</sup>, A. V. Ilyushechkina<sup>a</sup>, A. G. Kravchenko<sup>a</sup>, I. V. Kuz'min<sup>a</sup>, P. A. Kuchugov<sup>b,c</sup>,  
A. E. Myusova<sup>a</sup>, V. G. Rogachev<sup>a</sup>, A. N. Rukavishnikov<sup>a</sup>, E. Yu. Solomatina<sup>a</sup>, K. V. Starodubtsev<sup>a</sup>,  
P. V. Starodubtsev<sup>a</sup>, I. A. Chugrov<sup>a</sup>, O. O. Sharov<sup>a</sup>, and R. A. Yakhin<sup>b,\*</sup>

<sup>a</sup> All-Russia Research Institute of Experimental Physics, Russian Federal Nuclear Center,  
Sarov, Nizhny Novgorod oblast, 607188 Russia

<sup>b</sup> Lebedev Physical Institute, Russian Academy of Sciences, Moscow, 119991 Russia

<sup>c</sup> Keldysh Institute of Applied Mathematics, Russian Academy of Sciences, Moscow, 125047 Russia

\*e-mail: yakhin.rafael@gmail.com

Received October 14, 2021; revised October 14, 2021; accepted November 19, 2021

**Abstract**—Results of experiments aimed at amplification of the pressure of laser-induced shock wave on the passage from low- to high-density target material via vacuum gap are presented. During the action of nano-second laser pulse of terawatt power on plane composite targets comprising a layer of laser radiation absorber of low-density ( $0.01\text{--}0.025\text{ g/cm}^3$ ) spaced by vacuum gap from a layer of aluminum, the shock-wave velocity in aluminum reached  $25\text{--}29\text{ km/s}$  and a pressure jump at the aluminum layer boundary was  $1.2\text{--}1.5$  times as large as that observed in experiments on the cumulative transition of laser-induced shock wave into a solid. The obtained experimental data are compared to results of the numerical calculations performed using hydrodynamic programs in which the shock-wave generation and propagation was modeled with allowance for the interaction of laser pulses with partly homogenized plasma of the porous material. Based on the results of experiments, numerical calculations, and their theoretical analysis, the efficiency of using low-density porous media in the targets intended for their equation of state investigations and inertial confinement fusion ignition is considered.

DOI: 10.1134/S106377612203013X

### 1. INTRODUCTION

Shock wave generation as a result of the action of high-power laser radiation pulses on matter is among most remarkable phenomena in the high energy density physics. In practice, modern investigations in this field consist primarily in providing pressure buildup in the framework of the equation of state (EOS) studies of target materials and in realization of the inertial confinement fusion (ICF) conditions. Owing to a high energy flux density of laser radiation, laser-induced X-ray radiation, or laser-accelerated electron beam, modern laboratory experiments allowed record high pressures of quasi-stationary shock wave in a solid target to be achieved.

A traditional experimental approach consists in the direct exposure of a target to pulses of laser or laser-induced X-ray radiation. Pressures achieved using pulses of short-wave Nd laser of terawatt power amount to several dozen megabars [1–3]. A shock wave is generated due to the so-called laser ablation pressure that arises as a result of the evaporation and

thermal expansion (ablation) of matter from the irradiated target surface. Another method capable of significantly increasing the shock-wave pressure consists in energy concentration in the target as a result of the impact of a macroparticle accelerated due to the laser ablation. Using this “collisional” technique (more complicated for practical implementation) and terawatt Nd laser or laser-induced X-ray pulses, record high shock-wave pressures up to several hundred megabars have been achieved [4–7]. Moreover, there were theoretical and numerical calculations that justified the possibility of generating quasi-stationary shock waves with pressures up to several gigabars in targets under the action of relativistic electron beams accelerated in the field of petawatt laser radiation pulses [8, 9].

A universal method of increasing the shock-wave pressure is based on using its passage into a matter of higher density [10]. This approach can be considered as a variant of the “collisional” method in which the shock wave plays the role of accelerated macroparticle.

In the simplest scheme of experiment with laser ablation, this method is based on using a target comprising layers of different densities where the primary shock wave is generated due to the ablation of a layer with lower density. In particular, the low-density ablator of this target can represent a gas with the density above the critical value for plasma corresponding to the wavelength of laser radiation employed. However, this leads to significant complication of the technical realization of experiment, since the target must be either arranged in a gas-filled chamber with windows for diagnostics and laser beam entry or provided with walls surrounding this “gaseous” ablator and laser beam entry window.

A more appropriate material for the low-density ablator is offered by a porous substance (foam) based on light chemical elements. The physics of high-power laser radiation acting on porous materials is now extensively studied in view of the interest in fundamental phenomena of laser–plasma interaction important for some applied tasks, particularly, for the aforementioned ICF process [11, 12]. Porous materials have a number of important advantages in respect of the absorption of laser radiation and formation of the ablation pressure. One of these advantages is a highly efficient absorption of terawatt laser pulses. As established in numerous experiments, the energy fraction of first to third harmonics of Nd laser radiation absorbed within geometric transparency length of various porous materials based on light elements amounts to 80–90% for foams with both sub- and super-critical densities [13–18]. In addition, the absorption of laser radiation in a material of supercritical density ( $\rho > \rho_{cr}$ ) is a premise for developing ablation pressures on a level higher than that for the laser pulse action on solids in which the radiation can only be absorbed in plasma of subcritical density [19, 20]. Thus, a porous (foam) layer plays simultaneously the roles of (i) laser radiation absorber with minimum energy losses for self-radiation and (ii) ablator ensuring shock wave generation.

The energy transfer in partly homogenized plasma of a porous material is mediated by a hydrothermal wave [13] representing a shock wave with quasi-homogeneous temperature distribution behind the front and without ionization precursor ahead, which is caused by suppressed electron heat conductivity in view of the absence of free electrons in unperturbed porous material. The velocity of hydrothermal wave  $D_h$  is lower than that of shock wave  $D_s$  in the equivalent homogeneous medium of average density and chemical composition. This is related to delay in the pressure formation behind the hydrothermal wave as determined by

the time of porous material homogenization. For a terawatt laser pulse and a porous material with a density of  $(3–10)\rho_{cr}$ , the ratio  $D_h/D_s$  amounts to 0.7–0.5 [13, 14, 17, 20–25].

The phenomenon of shock-wave pressure buildup on the passage from low-density porous ablator into solid material has been studied in [26–28]. These experiments employed layered targets based on aluminum covered with a layer of porous  $C_{15}H_{20}O_6$  material (foam) with density varied in a broad range, which were irradiated by subnanosecond (400–600 ps) pulses of Nd-laser second-harmonic or I-laser third-harmonic radiation with intensity on the order of  $10^{14}$  W/cm<sup>2</sup>. The laser-induced shock-wave pressure in the aluminum layer exhibited 2.5-fold increase as compared to that in the porous layer.

In the present work, the approach based on the use of a target with porous ablator has been developed so as to enhance the “collisional” effect by separating the layers of porous ablator and solid part of the target with a vacuum gap. The second section of this article presents the results of experiments in which targets of this type were exposed to nanosecond pulses of second-harmonic radiation of terawatt Nd laser. The shock-wave velocity was measured in a solid layer of aluminum, while the porous absorber represented a layer of cellulose triacetate (CTA) based foam. Laser radiation pulses had 3.5–4 ns duration (full width at half-maximum, FWHM), which was 5–6 times greater than the values used in previous experiments [26–28]. In contrast to those, the longer pulse width allowed establishing a quasi-stationary regime of maximum pressure transfer from porous ablator to solid part of the target. The third section discusses the results of numerical modeling and considers the features of shock-wave generation and propagation in the porous ablator and solid part of a target.

## 2. EXPERIMENTAL

Experiments were performed in the All–Russia Research Institute of Experimental Physics at the Russian Federal Nuclear Center (RFNC, Sarov, Russia) on the LUCH laser fusion facility [29] using a method of high-speed laser plasma glow monitoring. Pulses of second-harmonic radiation of Nd phosphate glass laser with a wavelength of  $\lambda = 0.53$   $\mu$ m had a trap-ezoidal shape with FWHM of 3.4–3.8 ns, leading front width of 1.5–2.2 ns, and trailing front width of about 1 ns. Laser radiation was normally incident onto the surface of a composite target comprising layers of solid aluminum and porous material separated by a vacuum gap (Fig. 1). The aluminum part had the shape of  $\Delta_b = 20$   $\mu$ m thick base with a step of same thickness ( $h_s$ ) on the rear side.

The porous material represented foamed cellulose triacetate (CTA) with chemical formula  $(C_{12}H_{16}O_8)_n$  and a microstructure comprising fine porous network

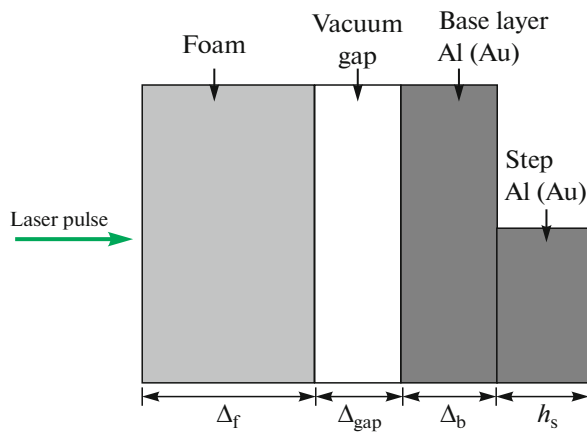


**Fig. 1.** Schematic diagram of a target comprising CTA foam layer and profiled solid aluminum layer spaced by a vacuum gap.

of crosslinked fibers (Fig. 2a). The CTA based foam was obtained by method of stimulated gelation in the (CTA–chloroform)/methanol system with a 1/2 volume ratio, followed by supercritical drying for aerogel formation. Blank foam layers were prepared by casting gel-forming polymer solution of preset concentration into a mold comprising flat gasket holder with planar glass walls, followed by cooling, solvent substitution, and supercritical drying in a special setup using carbon dioxide as extractant. The foam exhibited shrinkage (15–50% of the initial volume) on drying, thus forming a vacuum gap between porous and solid layers of the target. Geometric parameters of the foam blank upon drying and removal of the mold could be varied with the aid of Alicona Infinite Focus G5 optical 3D-profilometer. Figures 2b and 2c present photographs of assembled target as viewed from the frontal (foam) and rear (profiled aluminum) sides.

Targets were prepared with porous layers of variable density from 24 to 9 mg/cm<sup>3</sup>. Foam layers had approximately the same thickness (about 250 μm) significantly exceeding the geometric transparency length in the indicated interval of densities. The vacuum gap width was about one-third of the foam layer thickness, as selected so that to ensure, on one hand, noticeable enhancement of the “collisional” effect and, on the other hand, not too high rate of aluminum layer unloading and, hence, not too short duration of the quasi-stationary stage of shock-wave propagation in aluminum.

Experiments determined the moments of shock-wave escape from the base layer and step of aluminum. Then, the mean velocity of shock-wave propagation in the step was defined as the ratio of step thickness to the difference  $\Delta t$  of escape moments. Plasma glow on the rear surface of target was monitored with the aid of a streak camera (slit photochronograph) [30] which switched the electro-optical converter with an ultimate temporal resolution of 1 ps, photocathode with a working field size of  $h = 8$  mm, microchannel-plate image brightness amplifier, and digital CCD camera with 1000 × 1000 matrix. At a sweep rate of 10 ps per screen, the photochronograph could measure time intervals between the fronts of detected pulses with an error not exceeding 15 ns. A fraction of laser pulse radiation was directed via special optic-fiber channel onto the photochronograph slit so as to ensure temporal relation between the incident pulse and laser-induced shock-wave propagation process in the target.

Table 1 presents data on the parameters of laser pulses and targets, as well as mean shock-wave velocity in the step of aluminum layer as measured in three experimental laser shots. Laser radiation intensity on the target refers to the homogeneous part of laser spot with allowance for the transmittance of objective (measured in a series of experiments). The shock-wave velocity in Al layer step is given with an error including the



**Fig. 2.** Photographs showing (a) foam microstructure and (b, c) target viewed from the frontal (foam) and rear (profiled aluminum) sides, respectively.

**Table 1.** Experimental conditions and results of shock-wave velocity measurements in Al layer step ( $E_L$ , laser pulse energy on the target;  $\tau_{0.5}$ , pulse FWHM;  $\tau_1$ , pulse leading front width;  $\tau_2$ , pulse trailing front width;  $I_{Lm}$ , maximum radiation intensity on the target;  $\rho$ , TCA foam density;  $\Delta_f$ , foam layer thickness;  $\Delta_{gap}$ , vacuum gap width;  $D$ , shock-wave velocity in Al layer step)

Experiment	$E_L$ , J	$\tau_{0.5}$ , ns	$\tau_1$ , ns	$\tau_2$ , ns	$I_{Lm}$ , $10^{14}$ W/cm <sup>2</sup>	$\rho_f$ , g/cm <sup>3</sup>	$\Delta_f$ , $\mu$ m	$\Delta_{gap}$ , $\mu$ m	$D$ , km/s
1	230	3.4	2.2	1	0.16	0.024	275	87	$29.5 \pm 2.2$
2	190	3.8	1.5	0.9	0.11	0.011	242	72	$25.0 \pm 3.2$
3	240	3.45	1.7	0.8	0.15	0.009	241	92	$25.8 \pm 2.0$

uncertainty of step thickness, delay of the glow emission from the Al base layer and step, and spread of the plasma glow start (including the non-simultaneity of glow onset).

Figure 3 shows an example of the temporal variation of plasma glow intensity emitted from Al step in experiment 3 (see Table 1), in which the time delay between glow in the Al base layer and step amounted to  $\Delta t = 0.78$  ns.

### 3. NUMERICAL CALCULATIONS AND DISCUSSION OF RESULTS

Numerical calculations were performed for three groups of model targets: (i) 3 targets used in experiments presented in Table 1; (ii) 3 targets with the same porous ablator layers but not containing vacuum gaps; (iii) 3 targets without vacuum gaps but with homogeneous ablator layers of the same chemical composition, density and thickness as those indi-

cated in Table 1. The Al layer thickness was selected equal to 50  $\mu$ m, which allowed the complete pattern of shock-wave propagation in the Al base layer and step to be traced.

Numerical calculations for the targets with homogeneous ablators were performed using standard version of DIANA program package [31, 32]. Calculations for the targets with porous ablators employed DIANA-P program package that included a block for computation of the interaction of laser radiation with partly homogenized plasma of porous substance. This program ensured computation of the laser radiation absorption as a result of the bulk-retardation process in a region of with dimensions determined by the geometric transparency length [33, 34]. The geometric transparency length depends on the time of plasma homogenization in ion-ion collisions [34, 35]. The equations of motion and energy employ operators of limitation of the pressure gradient and electronic heat conductivity flux, respectively, which are also the functions of time- and coordinate-dependent plasma homogenization time [19, 35]. Parameters of the porous material structure were set by selecting the average pore size  $\delta_0$  (0.5  $\mu$ m for all targets under consideration) and unified fractal parameter [34, 35] set at  $\alpha = 0.8$  corresponding to the filamentary-membrane structure. The average thickness  $b_0$  of solid elements of the foam was selected based on the relation  $b_0 = \delta_0(\rho/\rho_s)^\alpha$  [34, 35], where  $\rho$  is the average foam density and  $\rho_s = 1.1$  g/cm<sup>3</sup> is the density of solid elements. This formula yields the values of  $b_0 = 0.025$ , 0.013, and 0.012  $\mu$ m corresponding to  $\rho = 0.024$ , 0.011, and 0.009 g/cm<sup>3</sup>, respectively. The density of homogeneous gas in the gap with the chemical composition equivalent to that of the porous ablator was selected at  $10^{-5}$  g/cm<sup>3</sup>.

Table 2 presents the results of calculations that refer to average values of the shock-wave pressure and velocity in target ablators, as well as in the Al base and step. In addition, calculations were also performed using codes adopted at the RFNC,

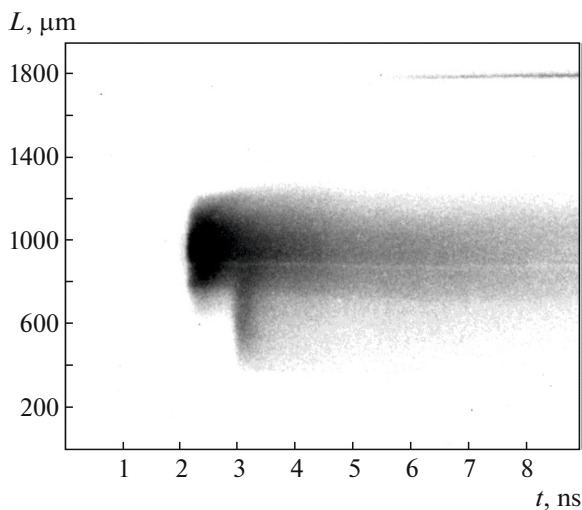


**Fig. 3.** Temporal variation of the plasma glow intensity in experiment 3 (see Table 1).

**Table 2.** Results of numerical model calculations of the ablation pressure in low-density absorber and the shock-wave pressure and velocity in Al base layer and step ( $P_{abl}$ , average pressure behind the shock-wave front in the ablator;  $D_{abl}$ , mean shock-wave velocity in the ablator;  $P_{base}$ , pressure in Al base layer;  $D_{base}$ , shock-wave velocity in Al base;  $P_{step}$ , shock-wave pressure in Al step;  $D_{step}$ , shock-wave velocity in Al step; \*asterisk indicates calculations for model targets with homogeneous ablators)

Model	$I_{Lm}, 10^{14}$ W/cm <sup>2</sup>	$\rho_f, \text{g/cm}^3$	$\Delta_f, \mu\text{m}$	$\Delta_{gap}, \mu\text{m}$	$P_{abl}$ , Mbar	$D_{abl}$ , km/s	$P_{base}$ , Mbar	$D_{base}$ , km/s	$P_{step}$ , Mbar	$D_{step}$ , km/s
1	0.16	0.024	275	87	3.5	110	18	30	16	28
2	0.16	0.024	275	0	3.5	110	18	30	11	23
3*	0.16	0.024	275	0	3.5	120	17	29	13	25
4	0.11	0.011	242	72	2.8	120	16	28	7	17
5	0.11	0.011	242	0	2.8	120	10	22	5	16
6*	0.11	0.011	242	0	2.8	130	12	24	6	18
7	0.154	0.009	241	92	3.5	150	13	26	7	18
8	0.154	0.009	241	0	3.5	150	12	24	6	17
9*	0.154	0.009	241	0	3.5	160	12	24	6	17

including those taking into account radiative heat transfer in the porous material and aluminum. Values obtained in these calculations are almost identical to those presented in Table 2 and are not considered separately.

Analysis of the data summarized in Table 2 allows the following conclusions to be made. All targets revealed cumulative amplification of the shock-wave pressure in aluminum in comparison to that in the ablator. This effect was most pronounced in targets with a vacuum gap between the ablator and aluminum layer. The growth of pressure in the Al base layer of various targets ranges from 3.5 to 6.3 times. The values of pressure behind the shock-wave front in the ablator (almost equal to the ablation pressures) exhibit rather insignificant differences in accordance with slightly different intensities of incident laser pulses. The values of ablation pressures fall in a range of 2.8–3.5 Mbar. The ablation pressure as dependent on the laser intensity for all targets can be evaluated using the well-known scaling relation [3, 36] established for the action of laser pulses on a substance with supercritical density ( $\rho > \rho_{cr}$ ). This is related to the fact that the employed ablator densities (11 and 9 mg/cm<sup>3</sup> in model calculations No. 5–8) are only 1.2 and 1.4 times lower than  $\rho_{cr}$ , so that laser radiation after shock-wave generation would act on the substance of supercritical density. Thus, the scaling relation for ablation pressures has the following form:

$$P_{abl}[\text{Mbar}] \approx \rho_{cr} \left( \frac{2(\gamma-1) I_L}{3\gamma-1 \rho_{cr}} \right)^{2/3} \quad (1)$$

$$\approx 12 \left[ \frac{2(\gamma-1)}{3\gamma-1} \right]^{2/3} \left( \frac{A}{Z} \right)^{1/3} \frac{I_{L(14)}^{2/3}}{\lambda_{\mu}^{2/3}},$$

where  $\rho_{cr} \approx 1.8 \times 10^{-3} A/Z\lambda_{\mu}^2$  is the critical density (in g/cm<sup>3</sup>);  $A$  and  $Z$  are the atomic number and degree of plasma ionization, respectively;  $\lambda_{\mu}$  is the wavelength (in microns);  $I_{L(14)}$  is the radiation intensity (in  $10^{14}$  W/cm<sup>2</sup> units); and  $\gamma$  is the adiabatic exponent.

In the approximation of fully ionized plasma in the evaporated part of ablator ( $A/Z \approx 2$ ,  $\gamma = 5/3$ ), estimations by formula (1) for  $\lambda_{\mu} = 0.53 \mu\text{m}$  with  $I_L = 0.16 \times 10^{14}$  W/cm<sup>2</sup> and  $I_L = 0.154 \times 10^{14}$  W/cm<sup>2</sup> yield  $P_{abl} = 3.2$  Mbar, and the estimation with  $I_L = 0.11 \times 10^{14}$  W/cm<sup>2</sup> yields  $P_{abl} = 2.5$  Mbar. These values are in good agreement with the results of numerical model calculations.

Approximate estimate of shock-wave pressure increase upon the passage from ablator with density  $\rho_{abl}$  into solid layer with density  $\rho_s$  is given by the following formula [28, 37]:

$$G \approx \left( \frac{1 + \beta^{1/2}}{1 + \beta^{1/2} \rho_{abl}/\rho_s} \right)^2,$$

where  $\beta = (1 + \gamma_{abl})$ ;  $\gamma_{abl}$  and  $\gamma_s$  are the adiabatic exponents in the ablator and target, respectively. For targets involving extended ablator with  $\rho_{abl} \ll \rho_s$ , this estimation yields a scale of pressure increase by a factor of about 4. In the numerical calculations performed with

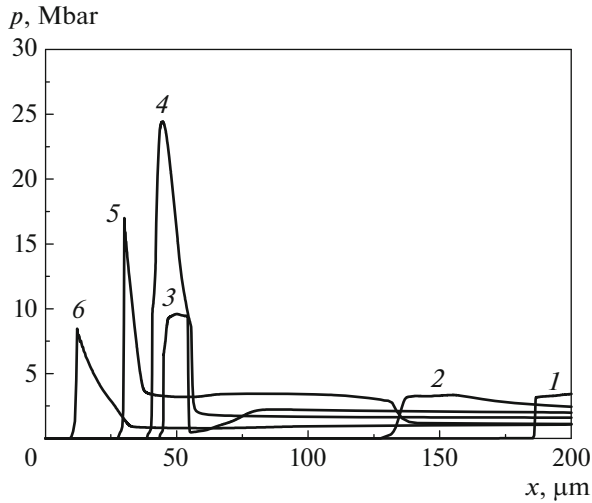


**Fig. 4.** Pressure profiles obtained in calculation No. 1 (Table 2) for a model target containing 50  $\mu\text{m}$  thick Al layer spaced by 87  $\mu\text{m}$  thick vacuum gap from 275  $\mu\text{m}$  thick porous layer with average density 24  $\text{mg}/\text{cm}^3$  irradiated by laser pulse of  $0.16 \times 10^{14} \text{ W}/\text{cm}^2$  intensity, as calculated at various moments of time  $t$  (ns): 3 (1); 3.5 (2); 4.2 (3); 4.4 (4); 4.75 (5); 5.45 (6).

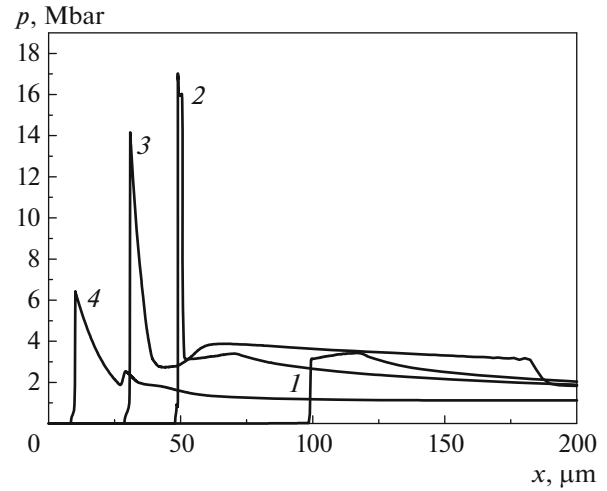


**Fig. 5.** Pressure profiles obtained in calculation No. 2 (Table 2) for a model target containing 50  $\mu\text{m}$  thick Al layer and 275  $\mu\text{m}$  thick porous ablator with average density 24  $\text{mg}/\text{cm}^3$  (without gap) irradiated by laser pulse of  $0.16 \times 10^{14} \text{ W}/\text{cm}^2$  intensity, as calculated at various moments of time  $t$  (ns): 3 (1); 3.5 (2); 4.1 (3); 5.0 (4).

allowance for the real EOS of aluminum in targets without vacuum gap, this factor ranges from 3.5 to 6.3, which corresponds to attaining pressures of 12, 10, and 18 Mbar in the Al base layer for targets with ablator densities of 9  $\text{mg}/\text{cm}^3$  (calculations No. 8 and 9 in Table 2), 11  $\text{mg}/\text{cm}^3$  (calculations No. 5 and 6), and 24  $\text{mg}/\text{cm}^3$  (calculations No. 2 and 3), respectively. The presence of a gap leads to about 30% shock-wave pressure increase in aluminum, whereby the pressure in Al step reaches 16 Mbar in the case of ablator with density 24  $\text{mg}/\text{cm}^3$  (calculation No. 1) and 7 Mbar for ablators with densities 11  $\text{mg}/\text{cm}^3$  (calculation No. 4) and 9  $\text{mg}/\text{cm}^3$  (calculation No. 7).

An important factor in applied tasks is related to the damping of shock waves in aluminum. In the given mode of experiments with approximately the same thickness of ablators, this damping is determined by the rate of ablator unloading: growth of the unloading rate leads to increase in the degree of shock-wave damping in aluminum. With allowance of Eq. (1), the isothermal sound velocity defined as  $V_s \approx (P_{\text{abl}}/\rho_{\text{abl}})^{1/2}$  amounts to

$$V_s \left[ \frac{\text{cm}}{\text{s}} \right] = \left( \frac{\rho_{\text{cr}}}{\rho_{\text{abl}}} \right)^{1/2} \left( \frac{2(\gamma-1) I_L}{3\gamma-1 \rho_{\text{cr}}} \right)^{1/3} \quad (2)$$

$$\approx 3.5 \times 10^6 \left[ \frac{2(\gamma-1)}{3\gamma-1} \right]^{1/3} \left( \frac{A}{Z} \right)^{1/6} \frac{I_L^{1/3}}{\lambda_{\mu}^{1/3} \rho_{\text{abl}}^{1/2}}.$$

According to this formula and the conditions of calculations No. 1, 2, and 3 (see Table 2) for ablators

with a density of 24  $\text{mg}/\text{cm}^3$  at laser pulse intensity  $I_L = 0.16 \times 10^{14} \text{ W}/\text{cm}^2$ , the sound velocity  $V_s$  is about 120 km/s. Under the conditions of calculations No. 4, 5, and 6 for the ablators with a density of 11  $\text{mg}/\text{cm}^3$  (2.2 times lower than in calculations No. 1, 2, and 3) at slightly reduced radiation intensity of  $I_L = 0.11 \times 10^{14} \text{ W}/\text{cm}^2$ , the sound velocity  $V_s$  amounts to about 160 km/s. Finally, under the conditions of calculations No. 7, 8, and 9 for the ablators with a density of 9  $\text{mg}/\text{cm}^3$  (2.7 times lower than in calculations No. 1, 2, and 3) and almost the same radiation intensity of  $I_L = 0.15 \times 10^{14} \text{ W}/\text{cm}^2$ , the sound velocity  $V_s$  reaches a maximum of about 200 km/s.

In the calculations for models No. 1, 2, and 3 with minimum  $V_s$  values, the rate of shock-wave damping in aluminum is also at minimum: mean velocities in the Al base layer and step are 29–30 and 23–28 km/s, respectively. Thus, the shock-wave velocity decrease in the step is about 5 km/s, i.e., 15% of the value in Al base layer. In this case, insignificant damping effect is confirmed by the following estimation. The time of ablator unloading can be evaluated as  $\Delta t/V_s \approx 2.3 \text{ ns}$ , during which the shock wave with average velocity 30 km/s would travel a distance of about 70  $\mu\text{m}$ , so that strong damping could be expected for Al layer thicknesses much greater than 40  $\mu\text{m}$ . In calculations No. 4, 5, and 6, the increase in  $V_s$  is accompanied by growth in the degree of shock-wave damping such that the wave velocities in the Al base layer and step are reduced to 22–28 and 16–18 km/s, respectively, and velocity decrease in the step (16–11 km/s) reaches

about 30% of the value in Al base layer. The time of ablator unloading in these calculations is about 1.5 ns, during which the shock wave with average velocity 21 km/s would travel a distance of about 30  $\mu\text{m}$ . Finally, calculations No. 7, 8, and 9 with maximum  $V_s$  value correspond to the maximum relative decrease in the shock-wave velocity: the average wave velocities in the Al base layer and step are 25 and 17 km/s, respectively, and velocity decrease in the step is about 30% of the value in Al base layer. The time of ablator unloading in these calculations is about 1.2 ns, during which the shock wave with average velocity 18 km/s would travel a distance of about 20  $\mu\text{m}$ . Thus, in calculations for the ablator density about 10 mg/cm<sup>3</sup>, the characteristic damping depths of 20–30  $\mu\text{m}$  turn out to be smaller than the Al layer thickness of 40  $\mu\text{m}$ , which is evidence of a rather strong damping of the shock wave.

Detailed temporal dynamics of the laser-induced shock-wave propagation is illustrated in Figs. 4, 5, and 6 showing pressure profiles calculated at various moments of time using models No. 1, 2, and 3 (Table 2) for targets with different ablators of same average density (24 mg/cm<sup>3</sup>):

- target with porous ablator and vacuum gap (model No. 1);
- target with porous ablator without vacuum gap (model No. 2);
- target with equivalent homogeneous ablator without gap (model No. 3).

In all calculations, the shock wave was generated by identical laser pulses with the same intensity ( $0.16 \times 10^{14}$  W/cm<sup>2</sup>). In calculation No. 3 for the model target containing homogeneous ablator without gap, the shock wave passes via 275  $\mu\text{m}$  thick ablator to reach the boundary of aluminum within  $t_{\text{abl}} \approx 2.8$  ns (Fig. 6), so that the average wave velocity in the homogeneous ablator is  $D_{\text{abl}} \approx 1.0 \times 10^7$  cm/s. At the moment of maximum laser pulse intensity ( $t = 2.2$  ns), the shock-wave velocity amounts to  $1.2 \times 10^7$  cm/s. Note that, for the ablation pressure of 3.5 Mbar, estimation of the shock-wave velocity by formula

$$D \approx [(\gamma + 1)P_{\text{abl}}/2\rho_{\text{abl}}]^{1/2}$$

yields a close value of  $D_{\text{abl}} \approx 1.4 \times 10^7$  cm/s.

In the porous ablator, the shock wave propagates (Figs. 4 and 5) much slower than in the equivalent homogeneous ablator due to the process of plasma homogenization. In the target without vacuum gap, the shock wave travels via ablator of the same thickness and reaches the boundary of aluminum for  $t_{\text{abl}} \approx$

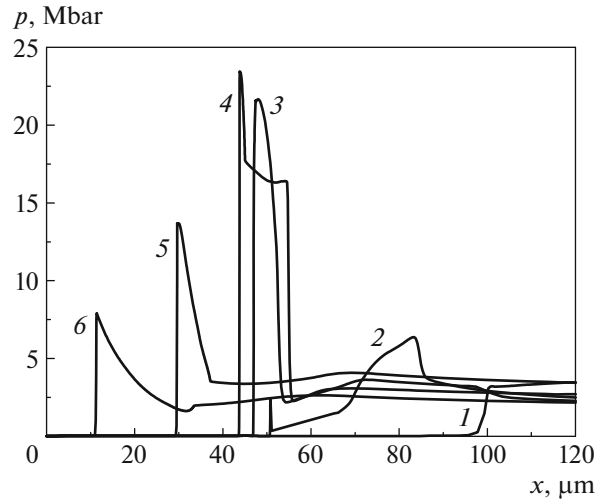


**Fig. 6.** Pressure profiles obtained in calculation No. 3 (Table 2) for a model target containing 50  $\mu\text{m}$  thick Al layer and 275  $\mu\text{m}$  thick homogeneous ablator with average density 24 mg/cm<sup>3</sup> (without gap) irradiated by laser pulse of  $0.16 \times 10^{14}$  W/cm<sup>2</sup> intensity, as calculated at various moments of time  $t$  (ns): 2.5 (1); 2.8 (2); 3.0 (3); 3.1 (4); 3.6 (5); 4.4 (6).

3.5 ns, so that the average velocity is about  $7 \times 10^6$  cm/s (Fig. 5). The time of plasma homogenization can be estimated using the following equation [34]:

$$\tau_h [\text{s}] \approx \frac{\delta_0}{V_i} \left[ 1 + \frac{\delta_0}{\lambda_{ii}} \right] \approx 3.3 \times 10^{-12} \frac{A^{1/2} \delta_0}{(Z+1)^{1/2} T^{1/2}} \times \left[ 1 + 7.3 \frac{Z^4 (Z+1)^{1/2} \delta_0 \rho}{AT^2} \right], \quad (3)$$

where  $\delta_0$  is the average pore size in microns,  $V_i$  is the thermal ion velocity,  $\lambda_{ii}$  is the ion–ion collision length,  $T$  [keV] is the plasma temperature, and  $\rho$  [g/cm<sup>3</sup>] is the average density of porous ablator.

In Eq. (3), the first term describes the time of primary pore filling and the second term refers to the density leveling by means of ion–ion collisions. For  $\delta_0 = 0.5$   $\mu\text{m}$ ,  $\rho = 0.024$  g/cm<sup>3</sup>,  $T = 1$  keV, and  $Z = 1$ , estimation of the plasma homogenization time yields about 1.5 ns. A similarity relationship for the velocity of shock-wave propagation in partly homogenized plasma of a porous substance is given by the following expression [25]:

$$D_h \left[ \frac{\text{cm}}{\text{s}} \right] \approx 9.7 \times 10^4 \frac{A^{2/3} I_L^{1/3}}{Z^{2/3} \lambda_{\mu}^{4/3} \rho^{\alpha} \rho_s^{1-\alpha}}. \quad (4)$$

For the fully ionized plasma in laser-irradiated porous target with parameters  $I_L = 0.16 \times 10^{14}$  W/cm<sup>2</sup>,  $\lambda = 0.53$   $\mu\text{m}$ ,  $\rho = 24$  mg/cm<sup>3</sup>,  $\rho_s = 1.1$  g/cm<sup>3</sup>, and  $\alpha =$

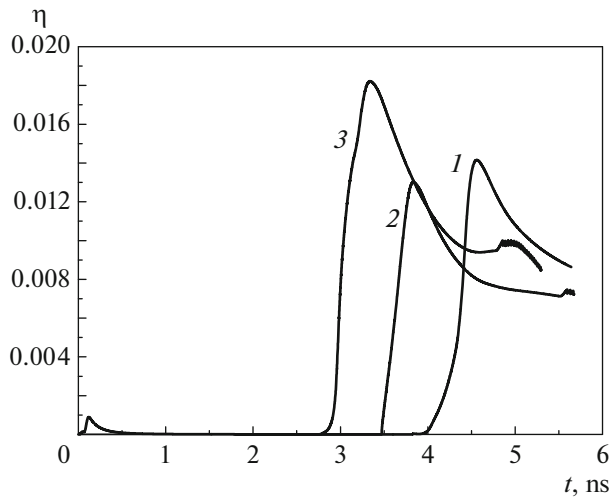


**Fig. 7.** Temporal variation of hydrodynamic efficiency  $\eta$  (ratio of the  $\eta$  kinetic energy of aluminum with density above initial to the absorbed laser energy) in targets with (1)  $24 \text{ g/cm}^3$  average density porous ablator with vacuum gap, (2) same porous ablator without gap, and (3) homogeneous ablator of same equivalent density without gap.

0.8, estimation of the shock-wave velocity by formula (4) yields a  $D_h$  value about  $5 \times 10^6 \text{ cm/s}$ . This estimation evidences, approximately to the same extent as the numerical calculations, much slower propagation of the laser-induced shock wave in a porous ablator as compared to the homogeneous one. In the case of a target with vacuum gap (Fig. 4), the formation of pressure on the Al layer surface equal to the laser-wave pressure in the ablator is due to plasma percolation via the vacuum gap, acceleration behind the shock-wave front, and retardation in the Al layer for a time of  $t_g \approx 0.5 \text{ ns}$ . For this reason, a powerful shock wave in Al layer in the target with vacuum gap is formed at a time of  $t_{abl} + t_g \approx 3.45 \text{ ns}$ . Simple estimation of the time of plasma percolation via  $87 \text{ }\mu\text{m}$  thick gap for the ablator substance moving behind the shock-wave front at a velocity of  $1.3 \times 10^7 \text{ cm/s}$  gives a value close to  $t_g \approx 0.6 \text{ ns}$ .

In the targets without gaps (Figs. 5 and 6), the pressures at which shock waves enter from the porous and homogeneous ablators into aluminum have close values about 18 Mbar and then slightly decrease within the first  $10 \text{ }\mu\text{m}$  of shock-wave passage in aluminum. The decrease grows but not significantly (to 14 Mbar) over the next  $10 \text{ }\mu\text{m}$  and then drop almost by half (to 7 Mbar) within the next  $20 \text{ }\mu\text{m}$  to attain a quasi-stationary regime of propagation at a pressure close to that in the ablator. In the target with porous ablator and vacuum gap (Fig. 4), the pressure at which the shock wave enters aluminum is about 26 Mbar, does not decrease in the first  $10 \text{ }\mu\text{m}$  of propagation, and then slightly decreases (to 15–17 Mbar) within the

next  $20\text{-}\mu\text{m}$  path. The pressure level of about 10 Mbar is retained even upon traveling over  $40 \text{ }\mu\text{m}$ . The rate of shock wave damping is rather correctly described by estimations presented above during the analysis of data summarized in Table 2.

Figure 7 shows calculated temporal profiles of hydrodynamic efficiency  $\eta$  of laser energy transfer to the shock wave, defined as the ratio of the kinetic energy of aluminum with density above initial to the laser energy absorbed in a target by the given moment of time. Maximum  $\eta$  values reach 1.28% at  $t = 3.3 \text{ ns}$  for the target containing porous ablator with vacuum gap, 1.42% at  $t = 3.8 \text{ ns}$  for the target containing same porous ablator without gap, and 1.82% at  $t = 4.5 \text{ ns}$  for the target with homogeneous ablator of same equivalent density without gap. The higher hydrodynamic efficiency observed for the target with homogeneous ablator is due to a lower energy absorbed in this ablator because the shock wave propagates without delay for the homogenization of plasma.

An important factor is the higher hydrodynamic efficiency observed for the target containing porous ablator with vacuum gap in comparison to the target with same porous ablator without the gap. Taking into account that greater laser energy is absorbed in the target with gap by the moment of energy transfer to the Al layer, this result is indicative of a greater energy transferred to Al layer during shock-wave impact via the vacuum gap.

At later stages of the shock wave propagation in aluminum, the hydrodynamic efficiency of both targets attains the “ablation” level of about 1%. The maximum values of  $\eta = 1.8\text{--}2.1\%$  are more than twice as large as those for the usual laser ablation regime of shock wave generation, whereby a laser pulse acts immediately on the surface of solid (e.g., aluminum) target [38]. It should be noted that the hydrodynamic efficiency of laser energy transfer in the ablation regime to shock-wave energy in a solid target is at least ten times lower than the efficiency of laser ablation acceleration of a thin planar layer of substance as a whole, which can reach (at the optimum dose of ablated mass about 80%) up to 38% [3, 36, 39].

Comparative scaling analysis of reported experimental data [26, 28] showed that experiments performed in the present work under equivalent conditions in respect of the laser pulse intensity and foam characteristics gave much higher values of the shock-wave velocity in aluminum. Indeed, shock waves generated by laser pulses of  $I_L \approx 0.5 \times 10^{14} \text{ W/cm}^2$  intensity and 600 ps duration in earlier experiments with foam–aluminum targets at absorber densities of 10 and  $20 \text{ mg/cm}^3$  [26, 28] had velocities of 22–24 and 22–26 km/s, respectively, at 13–18  $\mu\text{m}$  depth in aluminum. Taking into account the scaling relation for ablation pressure,  $P_{abl} \propto I_L^{2/3}$ , and the laser pulse intensity of  $I_L \approx 0.15 \times 10^{14} \text{ W/cm}^2$  used in the present work,



those values would correspond to 16–17 and 16–18.5 km/s, respectively. Thus, shock-wave velocities of about 25 and 29 km/s observed in aluminum at a greater depth of 20–40  $\mu\text{m}$  in our experiments exceed the scaled values reported in [26, 28] by a factor of about 1.5.

There are two possible reasons for this difference. First, the much longer duration of laser pulses that ensures maximum ablation pressure achieved during the entire process of shock wave propagation in the porous ablator and aluminum layer. Second, the presence of vacuum gap between the ablator and aluminum, which ensures attaining the maximum efficiency of shock-wave energy transfer to aluminum as confirmed by the results of numerical calculations

#### 4. CONCLUSIONS

In these experiments, nanosecond laser pulses of  $(1-1.5) \times 10^{13} \text{ W/cm}^2$  intensity acting upon planar targets comprising a layer of low-density porous ablator-absorber (10–25  $\text{mg/cm}^3$ ) spaced by vacuum gap from a layer of aluminum generated shock waves with velocities 25–29 km/s in aluminum. Analysis of the experimental results with the aid of numerical calculations modeling the generation and propagation of shock waves in partly homogenized laser plasma of porous (foam) ablator showed that the main factor ensuring the attainment of high shock-wave velocities are (i) the presence of a vacuum gap that provides 1.2–1.5 fold amplification of the shock-wave pressure in aluminum and (ii) optimum duration (about 4 ns) of the laser pulse that ensures maximum ablation pressure in the porous absorber during the entire process of shock-wave propagation in the ablator and aluminum layers of target.

In view of the scaling relation for initiating ablation pressures,  $P_{\text{abl}} \propto I_L^{2/3}$ , a tenfold increase in laser pulse intensity and the passage to third harmonic can be expected to produce an eight-fold growth in shock-wave pressure (up to 200–250 Mbar) in the solid target and about 2.8-fold growth in shock-wave velocity (up to  $8-9 \times 10^6 \text{ cm/s}$ ), which is a quite serious result for EOS experiments with planar targets under standard conditions of pulsed laser irradiation.

Finally, it should be noted that the length of quasi-stationary shock-wave propagation in aluminum (about 10  $\mu\text{m}$ ) corresponds to a distance of about 30  $\mu\text{m}$  in plastics (a typical solid-plastic ablator thickness in direct-ignition ICF targets [3, 40, 41]). This implies that the use of composite ablators comprising solid plastic and porous substance layers can lead not only to increase in the efficiency of laser radiation absorption and leveling of ICF target irradiation inhomogeneity, but also to increase in hydrodynamic efficiency of the absorbed laser energy transfer to the target.

#### CONFLICT OF INTEREST

The authors declare that they have no conflicts of interest.

#### REFERENCES

1. S. G. Garanin, *Phys. Usp.* **54**, 415 (2011).
2. R. S. Craxton, K. S. Anderson, T. R. Boehly, et al., *Phys. Plasmas* **22**, 110501 (2015).
3. J. Lindl, *Phys. Plasmas* **2**, 3933 (1995).
4. R. Cauble, D. W. Phillion, T. J. Hoover, et al., *Phys. Rev. Lett.* **70**, 2102 (1993).
5. M. Karasik, J. L. Weaver, Y. Aglitskiy, et al., *Phys. Plasmas* **17**, 056317 (2010).
6. T. Watari, T. Sakaiya, H. Azechi, et al., *J. Phys.: Conf. Ser.* **112**, 022065 (2008).
7. M. Murakami, H. Nagatomo, T. Johzaki, et al., *Nucl. Fusion* **54**, 054007 (2014).
8. S. Yu. Gus'kov, *JETP Lett.* **100**, 71 (2014).
9. S. Yu. Gus'kov, P. A. Kuchugov, and G. A. Vergunova, *Matter Radiat. Extrem.* **6**, 020301 (2021).
10. Ya. B. Zel'dovich and Yu. P. Raizer, *Physics of Shock Waves and High-Temperature Hydrodynamic Phenomena* (Fizmatlit, Moscow, 2008; Academic, New York, 1966, 1967).
11. S. Yu. Gus'kov, N. V. Zmitrienko, and V. B. Rozanov, *Zh. Eksp. Teor. Fiz.* **108**, 296 (1995).
12. A. S. Moore, N. B. Meezan, C. A. Thomas, et al., *Phys. Plasmas* **27**, 082706 (2020).
13. A. E. Bugrov, I. N. Burdonskii, V. V. Gavrilov, et al., *Laser Part. Beams* **17**, 415 (1999).
14. Ph. Nicolai, M. Olazabal-Loume, S. Fujioka, et al., *Phys. Plasmas* **19**, 113105 (2012).
15. S. Depierreux, C. Labaune, D. Michel, et al., *Phys. Rev. Lett.* **102**, 195005 (2009).
16. M. Tanabe, H. Nishimura, S. Fujioka, et al., *Appl. Phys. Lett.* **93**, 051505 (2008).
17. A. Caruso, C. Strangio, S. Yu. Gus'kov, et al., *Laser Part. Beams* **18**, 25 (2000).
18. T. Hall, D. Batani, W. Nazarov, et al., *Laser Part. Beams* **20**, 303 (2002).
19. S. Yu. Gus'kov, M. Cipriani, R. de Angelis, et al., *Plasma Phys. Control. Fusion* **57**, 125004 (2015).
20. R. de Angelis, F. Consoli, S. Yu. Gus'kov, et al., *Phys. Plasmas* **22**, 072701 (2015).
21. A. E. Bugrov, I. N. Burdonskii, V. V. Gavrilov, et al., *J. Exp. Theor. Phys.* **84**, 272 (1997).
22. M. Cipriani, S. Yu. Gus'kov, R. de Angelis, et al., *Phys. Plasmas* **25**, 092704 (2018).
23. J. D. Colvin, H. Matsukuma, K. C. Brown, et al., *Phys. Plasmas* **25**, 032702 (2018).
24. J. Velechovsky, J. Limpouch, R. Liska, and V. Tikhonchuk, *Plasma Phys. Control. Fusion* **58**, 095004 (2016).
25. S. Yu. Gus'kov, J. Limpouch, Ph. Nicolai, and V. T. Tikhonchuk, *Phys. Plasmas* **18**, 103114 (2011).
26. A. Benuzzi, M. Koenig, B. Faral, et al., *Phys. Plasmas* **5**, 2410 (1998).
27. M. Temporal, S. Atzeni, D. Batani, et al., *Eur. Phys. J. D* **12**, 509 (2000).

28. D. Batani, A. Balducci, W. Nazarov, et al., *Phys. Rev. E* **63**, 046410 (2001).
29. S. G. Garanin, A. I. Zaretskii, R. I. Il'kaev, et al., *Quantum Electron.* **35**, 299 (2005).
30. D. S. Kornienko, A. G. Kravchenko, D. N. Litvin, V. V. Mis'ko, A. N. Rukavishnikov, A. V. Senik, K. V. Starodubtsev, V. M. Tarakanov, and A. E. Chaunin, *Instrum. Exp. Tech.* **57**, 165 (2014).
31. N. V. Zmitrenko, V. Ya. Karpov, A. P. Fadeev, et al., *Vopr. At. Nauki Tekh., Ser.: Metod. Progr. Chisl. Reshen. Zadach At. Fiz.*, No. 2, 34 (1983).
32. S. Yu. Gus'kov, P. A. Kuchugov, R. A. Yakhin, et al., *Plasma Phys. Control. Fusion* **61**, 105014 (2019).
33. S. Yu. Gus'kov and V. B. Rozanov, *Quantum Electron.* **27**, 696 (1997).
34. S. Yu. Gus'kov and J. Russ, *Laser Res.* **31**, 574 (2010).
35. M. Cipriani, S. Yu. Gus'kov, R. de Angelis, et al., *Laser Part. Beams* **36**, 121 (2018).
36. Yu. V. Afanasiev and S. Yu. Gus'kov, in *Nuclear Fusion by Inertial Confinement. A Comprehensive Treatise*, Ed. by G. Velarde, Y. Ronen, and J. M. Martinez-Val (CRC Press, Boca Raton, 1992), Chap. 4.
37. S. Yu. Gus'kov, H. Azechi, N. N. Demchenko, et al., *Plasma Phys. Control. Fusion* **51**, 095001 (2009).
38. S. Yu. Gus'kov, S. Borodzyuk, M. Kalal, et al., *Quantum Electron.* **34**, 989 (2004).
39. Yu. V. Afanas'ev, E. G. Gamalii, O. N. Krokhin, et al., *Prikl. Mat. Mekh.* **39**, 451 (1975).
40. V. B. Rozanov, C. P. Verdon, M. Decroisette, et al., in *Energy from Inertial Fusion*, Ed. by W. J. Hogan (IAEA, Vienna, 1995), p. 21.
41. S. A. Bel'kov, S. V. Bondarenko, G. A. Vergunova, S. G. Garanin, S. Yu. Gus'kov, N. N. Demchenko, I. Ya. Doskoch, P. A. Kuchugov, N. V. Zmitrenko, V. B. Rozanov, R. V. Stepanov, and R. A. Yakhin, *J. Exp. Theor. Phys.* **121**, 686 (2015).

*Translated by P. Pozdeev*